Journal of Materials Chemistry A

Performance and Durability of Anion Exchange Membrane Water Electrolyzers using Down-selected Polymer Electrolytes

Journal:	*Journal of Materials Chemistry A*
Manuscript ID	TA-ART-08-2021-006869.R1
Article Type:	Paper
Date Submitted by the Author:	09-Sep-2021
Complete List of Authors:	Motz, Andrew; Nel Hydrogen, Li, Dongguo; Los Alamos National Laboratory, Materials Science Division Keane, Alex; Nel Hydrogen Delfin Manriquez, Luis; Los Alamos National Laboratory, Park, Eun Joo; Los Alamos National Laboratory, Maurya, Sandip; Los Alamos National Laboratory, MPA-11: Materials Synthesis and Integrated Devices Chung, Hoon; Los Alamos National Laboratory Fujimoto, Cy; Sandia National Laboratories , Organic Materials Jeon, Jong Yeob; Rensselaer Polytechnic Institute, Department of Chemistry and Chemical Biology Pagels, Michael; Rensselaer Polytechnic Institute Bae, Chulsung; Rensselaer Polytechnic Institute, Chemistry and Chemical Biology Ayers, Kathy; Nel Hydrogen Kim, Yu Seung; Los Alamos National Laboratory,

Performance and Durability of Anion Exchange Membrane Water Electrolyzers using Down-selected Polymer Electrolytes

Andrew R. Motz,[1⊥] Dongguo Li,[2⊥] Alex Keane,[1] Luis Delfin Manriquez,[2] Eun Joo Park,[2] Sandip Maurya,[2] Hoon Chung,[2ξ] Cy Fujimoto,[3] Jongyeob Jeon,[4] Michael K. Pagels,[4] Chulsung Bae,[4] Katherine E. Ayers,[1] and Yu Seung Kim[2*]

[1] Nel Hydrogen, Wallingford, CT, 06492, USA

[2] MPA-11: Materials Synthesis & Integrated Devices, Los Alamos National Laboratory, Los Alamos, New Mexico, 87545, USA

[3] Nanoscale Science Department, Sandia National Laboratories, Albuquerque, New Mexico, 87185, USA

[4] Department of Chemistry and Chemical Biology, Rensselaer Polytechnic Institute, Troy, New York, 12180, USA

[⊥] Equal contribution.

[ξ] Present address: Hanwha Solutions, Daejeon, Korea.

E-mail: yskim@lanl.gov (Y.S. Kim)

ABSTRACT

Over the last decade, several stable anion exchange polymer electrolytes have been developed for electrochemical devices. Herein, we investigate how chemical structure and physical properties of polymer electrolytes affect performance and durability of anion exchange membrane water electrolyzers (AEMWEs). We select polymer electrolytes with high alkaline stability and consider their polymer properties including conductivity, mechanical/chemical stability, and material interactions to interpret the performance and durability of AEMWEs. The AEMWE with a poly(phenylene) membrane and a poly(fluorene) ionomeric binder exhibited the best performance among those tested in this study; the AEMWE showed ~1 A cm^{-2} at 2 V under 1 wt% K_2CO_3-fed conditions. The voltage degradation rate was 270 - 550 $\mu V\ h^{-1}$ for several hundred operating hours at a constant current density of 750 mA cm^{-2} and a differential pressure of 100 pounds per square inch gauge. Based on these results, we discuss research needs of polymer electrolytes for practical AEMWEs.

INTRODUCTION

Hydrogen is an attractive energy storage material because of its high-energy storage capability and ability to conveniently generate electricity by carbon-neutral pathways, i.e., fuel cells.[1] Water is considered one of the most promising resources to produce hydrogen via renewable energy. Solid-oxide steam electrolyzer cells provide high energy efficiency (~ 100% $_{\text{High Heating Value}}$ at current densities of ~ 1 A cm^{-2});[2] however, problems associated with high-temperature operations make the use of solid-oxide electrolyzers challenging when deployed in large-scale commercial hydrogen production.[2] For low-temperature water electrolysis, an alkaline water electrolyzer is a well-established technology, but its hydrogen production rate is typically low (~ 0.2 A cm^{-2} at 1.8 V).[3] Proton exchange membrane water electrolyzers (PEMWEs) allow a zero-gap configuration at both the anode and cathode that are in physical contact with a non-porous proton exchange membrane which results in low ohmic resistance and enables operation at higher current densities when compared to alkaline water electrolyzers (≥ 2 A cm^{-2} at 2 V).[4] Furthermore, the non-porous membrane of PEMWEs allows differential pressure operations that produce high-pressure hydrogen at the cathode and atmospheric pressure oxygen at the anode. Such differential pressure operations can minimize the need for additional mechanical compression for hydrogen use or storage. Although PEMWE is considered a mature technology, the high costs of electrocatalysts, corrosion-resistant current collectors, and separator plates for PEMWEs become increasingly important on the multi-MW scale when the stack cost is a larger portion of the overall system cost.[5]

Anion exchange membrane water electrolyzers (AEMWEs) can also produce hydrogen under differential pressure conditions thus minimize the need for mechanical compression for hydrogen use or storage, similar to PEMWEs, as non-porous membranes are used. Additionally, less expensive components including platinum group-metal-free (PGM-free) electrocatalysts and

cheap bipolar plates made from stainless steel, nickel, surface-treated iron or graphite can be used under high pH conditions similar to alkaline water electrolyzers.[6, 7] All these advantages, low cost of catalysts/hardware, applicable zero-gap configurations, and differential pressure operation capability, make interest in hydrogen production via AEMWEs fast-growing.[8] As a result, tremendous technological progress has been made in anion exchange materials for PGM-free AEMWEs over the past several years. **Table 1** shows the selected anion exchange membranes (AEMs) and ionomers (AEIs) that enable the high performance of AEMWEs under specific testing conditions. These reports indicate that the high performance of PGM-free catalyzed AEMWEs (> 1 A cm^{-2} at 1.8 V) are feasible with state-of-the-art anion exchange materials, although the performance of AEMWEs is still inferior to those of benchmark PEMWEs.

Table 1. Comparison of materials and operating conditions between the benchmark PEMWE and selected AEMWE MEAs.

Electrolyzer	Membrane [a]		Ionomer Type	Operating Temp. (°C) /Diff. Pres. (bar)	Electrolyte	Catalyst		*i* (A cm^{-2}) @1.8 V	Ref.
	Type	Thickness (μm)				anode	cathode		
PEM	PFSA	178	PFSA	80/30	Polymer	Ir	Pt/C	1.6	13
	PFSA	51	PFSA	80/30	Polymer	Ir	Pt/C	3.5	13
AEM	Poly(phenylene)	26	Polystyrene	85/ambient	Polymer	NiFe	NiMo	0.9	14
	Poly(phenylene)	26	Polystyrene	85/ambient	Polymer	NiFe	PtRu	2.7	14
	Poly(aryl piperidinium)	20	Poly(aryl piperidinium)	90/ambient	Polymer	FeNiOOH-20F	Pt/C	1.0	15
	Polybenzimidazole	50	No ionomer[b]	60/ambient	1 M KOH	NiAlMo	NiAlMo	0.9	7
	Polybenzimidazole	40		80/ambient	24% KOH	Raney Ni	Raney NiMo	1.7	16
	Polystyrene	50	PFSA[c]	80/ambient	1 M KOH	Fe-NiMo-NH_3/H_2	NiMo-NH_3/H_2	1.0 @1.57 V	17

[a] non-reinforced
[b] prepared electrode by plasma spraying
[c] used as a binder

It should also be noted that the high performance of AEMWEs was only demonstrated either with a very thin membrane (thickness, t < 30 μm) or with the help of an additional circulating KOH electrolyte under ambient pressure conditions. While the use of a thin membrane offers a high potential for reducing hydrogen generation costs,[4] diffusion-driven hydrogen permeation through

a thin membrane would be a concern from a product reliability standpoint. High permeation of hydrogen not only reduces the faradaic efficiency of the electrolyzer but can also lead to the formation of explosive gas mixtures in the anode compartment.[9] The hydrogen permeation rate can substantially increase with the differential pressure operation due to the higher hydrogen partial pressure at the cathode compartment. Nevertheless, performance evaluation of AEMWEs using a thin AEM under differential pressure conditions is extremely rare; only one out of 61 AEMWE-related papers[10] published in 2020 reported on AEMWE performance under differential pressure conditions according to the literature analysis by Journal Citation Reports. Considering that the degradation pathways of polymer electrolytes can be different under differential pressure conditions,[11] the lack of studies on AEM failure under differential pressure conditions brings uncertainty in implementing the current AEMWE technology into a practical hydrogen production system. Boosting AEMWE performance with the aid of KOH solution brings another concern for device durability and system design complexity. Although perfluorosulfonic acid (PFSA) polymer electrolytes work well for PEMWEs without additional liquid electrolytes, the necessity of liquid electrolytes for AEMWEs is still arguable. There are two approaches to mitigate the adverse impact of using corrosive KOH solutions. The first approach is to develop more advanced ionomers that can completely replace liquid electrolytes and enable AEMWE operation under pure water-fed conditions. The second approach is to use a less-corrosive potassium carbonate solution instead of a KOH solution. For the second approach, it is believed that a potassium carbonate solution can provide a good compromise between a hydrogen production rate and device durability.[12]

In this study, our purpose is to demonstrate the performance and durability of AEMWEs using AEMs and AEIs down-selected after considering the shortcomings of AEMWEs. First, we down-

select AEMs based on their chemical stability and mechanical and electrochemical standpoints for the use of AEMWEs under differential pressure conditions. We compare the AEMWE performance of a single cell having AEMs with different chemical structures to determine the required minimum AEM thickness for long-term operation. Second, we investigate the performance-limiting factor of AEIs, focusing the chemical structure effect of AEIs on catalyst-ionomer interactions to down-select the best performing AEIs. Third, we demonstrate AEMWE durability using down-selected AEMs and AEIs under K_2CO_3-fed and 100 psig (6.9 bar) differential pressure conditions. While 30 bar H_2 is the current industry standard for PEMWEs, moderate pressure offers some benefits over ambient pressure operations including sufficient pressure for some process needs dependent on the requirements of the end-user, some reduction in compression requirements, and higher purity H_2 through reduced O_2 diffusion across the membrane. Finally, we discuss future R&D directions on AEM and AEI development for practical AEMWE systems based on performance and durability evaluation.

RESULTS AND DISCUSSION

Selection of anion exchange membranes and their properties

The chemical stability of AEMs under high pH conditions is one of the paramount requirements for AEMWE's performance and durability. The chemical stability of quaternized polymers under high pH conditions is well-documented.[18-20] In many cases, nucleophilic hydroxide attack starts with the cationic functional groups of quaternized polymers. It is known that alkyl ammonium cationic groups placed on pendant electron-donating alkyl spacer chains ($C > 4$) along the backbone improve the alkaline stability of the quaternary ammonium groups.[21-23] Stabilized imidazolium[24, 25] and piperidinium[26-28] cations have also been suggested as alternative cationic functional groups with enhanced alkaline stability. Those alkaline stable cationic functional groups

can survive without degradation for several thousands of hours under high pH conditions (0.5 - 4 M KOH solution) at typical AEMWE operating temperatures (50 - 80 °C). In other cases, aryl ether cleavage in the polymer backbone by nucleophilic hydroxide attack shortens the device's lifetime.[29-31] Unlike cationic group degradation, the polymer backbone degradation causes a catastrophic failure of device performance through crack propagation or membrane pinhole formation. Although a stable performance of alkaline AEM fuel cells using an aryl ether-containing AEM was demonstrated at 60 °C for 540 hours in a recent paper,[32] the majority of long-term performances (> 500 hours) of AEM-based electrochemical devices have been achieved with aryl ether-free quaternized polymers.[33-38] Therefore, we select chemically stable AEMs, and their performance is evaluated in MEAs for this study.

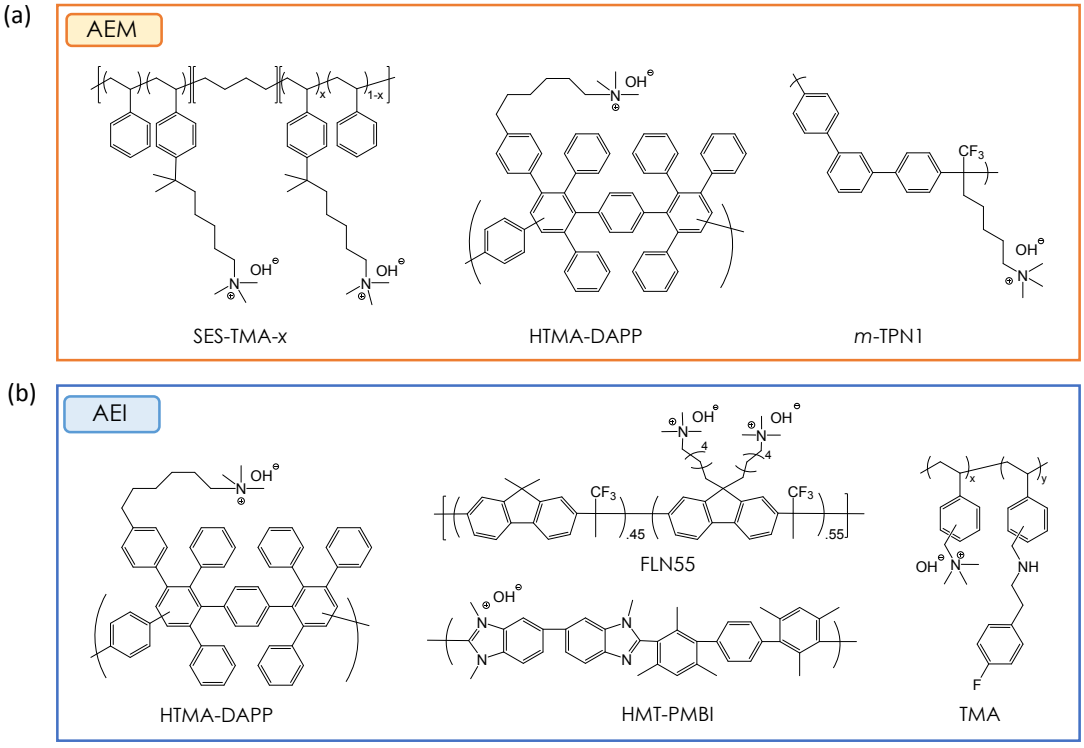

Figure 1. Chemical structure of AEMs and AEIs used for this study.

Considering the chemical stability aspects, we investigate three AEMs having aryl ether-free polymer backbones with alkyl ammonium pendant groups for this study. The chemical structures of AEMs are shown in **Figure 1a**. The first AEM is an alkyl trimethyl ammonium functionalized poly(styrene-ethylene-styrene) block copolymer (SES-TMA-*x*, *x* = ion exchange capacity (IEC)). The SES-TMA AEMs were prepared by acid-catalyzed Friedel-Crafts alkylation of the polystyrene block of SES-TMA using bromoalkylated tertiary alcohols and triflic acid as a catalyst, followed by amination with trimethylamine.[39] We prepared the SES-TMAs with two different IECs (1.4 and 1.7 mequiv. g^{-1}). The SES-TMA block copolymers are semi-crystalline (degree of crystallinity = 21% for SES-TMA-1.7) which provides good mechanical properties without crosslinking. The second AEM is an alkyl trimethyl ammonium functionalized Diels-Alder poly(phenylene) (HTMA-DAPP). The HTMA-DAPP AEM was prepared by reacting Diels-Alder poly(phenylene) with 6-bromohexanoyl chloride in the presence of aluminum chloride. The ketone group of the polymer was reduced to a methylene group by a reaction with trifluoroacetic acid and triethylsilane, followed by amination.[21] The third AEM is a polytetrafluoroethylene (PTFE) reinforced alkyl ammonium tethered poly(*meta*-terphenylene) (*m*-TPN1). This reinforced AEM was commercially available (Durion™, Xergy). The *m*-TPN1 polymer was prepared by the acid-catalyzed polycondensation.[40]

Table 2 shows the IEC, hydroxide conductivity (σ), water uptake (WU), and alkaline stability of the AEMs used for this study. The two poly(phenylene) AEMs (HTMA-DAPP and Durion) have lower water uptake but higher hydroxide conductivity than polystyrene-based polyolefinic AEMs (SES-TMA-*x*). The alkaline stability of the selected AEMs was evaluated with a concentrated NaOH solution at 80 °C after 300 to 1,000 hours. No conductivity changes were observed for SES-TMA-1.7 and *m*-TPN1 (hydroxide conducting resin for Durion) after the alkaline stability test with

1 M NaOH treatment at 80 °C. For HTMA-DAPP, the conductivity decreased from 119 to 89 mS cm^{-1} after the first 500-hour stability test with 4 M NaOH treatment 80 °C. The reduced conductivity of HTMA-DAPP was maintained for an additional 500-hours of alkaline stability testing, indicating that the initial conductivity decrease was not sustained. The reduction of conductivity of HTMA-DAPP is hypothesized to be due to the cross-linking of unreacted alkyl bromides of HTMA-DAPP through Williamson ether synthesis.[41] These results suggested that all AEMs used for this study have good chemical stability under high pH conditions.

Table 2. Electrochemical properties and alkaline stability of the quaternized AEMs used for this study.

AEM type	AEM	IEC [a] (mequiv./g^{-1})	WU [a] (%)	σ at 50 °C (mS cm^{-1})		σ_{OH^-} after alkaline stability test (mS cm^{-1})	
				OH^- form	carbonate form	Before	After
Polystyrene	SES-TMA-1.4	1.4	100	50 ± 1.2	13 ± 0.3	Not available	
Polystyrene	SES-TMA-1.7	1.7	144	61 ± 0.5	17 ± 0.3	63	64 [c]
Poly(phenylene)	HTMA-DAPP	1.5	98	90 ± 1.3	23 ± 0.4	119	88 [d]
Reinforced	Durion	2.0 – 2.3 [b]	88	87 ± 3.2	20 ± 0.3	127 [b]	125 [b, e]

[a] measured with OH^- form membranes
[b] measured without the reinforcing agent.
[c] tested SES-TMA for 300 hours of 1 M NaOH treatment at 80 °C.
[d] tested HTMA-DAPP for 1,000 hours of 4 M NaOH treatment at 80 °C. Data were taken from Ref.[41].
[e] tested *m*-TPN1 resin for 500 hours of 1 M NaOH treatment at 80 °C. Data were taken from Ref.[42].

We evaluated the mechanical properties of the selected AEMs at 50 °C in controlled relative humidity (RH) environments. **Figure 2** shows that SES-TMA AEMs have low modulus and strength but high elongation. There are negligible differences in mechanical properties between the low and high IEC SES-TMA AEMs. These SES-TMA AEMs were not disintegrated until it reached the instrumental limit. The tensile energy of the AEMs obtained from the area under the stress-strain curve was > 8.5 MPa at 80% RH (**Table 2**). In contrast, the HTMA-DAPP AEM had high modulus and strength but low elongation. Due to the low elongation, the tensile energy of the HTMA-DAPP AEM (2.3 MPa) was less than 30% of the SES-TMA at 80% RH. The reinforced Durion AEM showed similar stress-strain behavior of the HTMA-DAPP with notably higher strength (~14 MPa) as the PTFE reinforcement increases the resistance to deformation of the AEM.

The tensile energy of the Durion AEM (2.9 MPa) is slightly higher than that of HTMA-DAPP, but significantly lower than SES-TMAs. We also evaluated the mechanical properties of AEMs under dry condition of 10% RH. A similar stress-strain trend among the SES-TMA, HTMA-DAPP, and Durion was observed; high strength and modulus for Durion and HTMA-DAPP and high elongation for SES-TMA-1.4. **Table 3** summarizes the tensile properties of the AEMs. The tensile strength and modulus of the poly(phenylene) AEMs are higher than those of the poly(styrene)-based AEMs under all tested RH conditions, while the tensile energy of the poly(phenylene) AEMs is much lower because of low elongation.

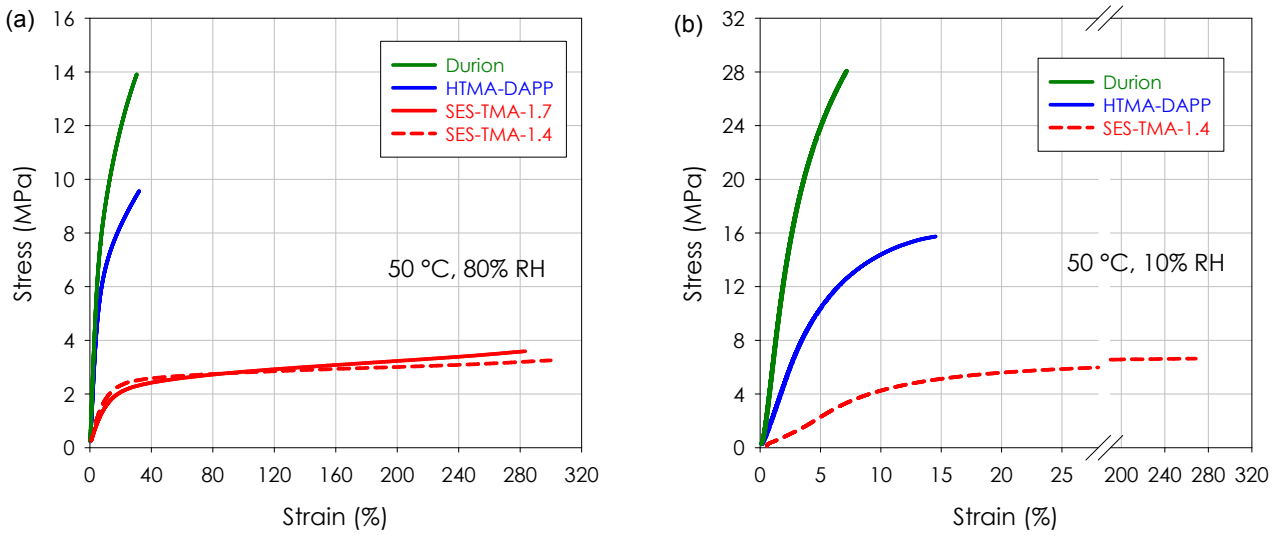

Figure 2. Stress-strain curves of AEMs at 50 °C. (a) 80% and (b) 10% RH.

Table 3. Tensile properties of the selected quaternized AEMs (OH^- form) at 50 °C.

AEM	% RH	Tensile modulus (MPa)	Tensile strength (MPa)	Elongation at break (%)	Tensile energy [a] (MPa)
SES-TMA-1.4	10	48	6.6	> 280	> 16.8
	50	44	6.5	> 280	> 18.2
	80	16	3.3	> 280	> 8.5
SES-TMA-1.7	80	16	3.6	> 280	> 8.2
HTMA-DAPP	10	252	15.7	14.5	1.6
	50	145	11.9	19.1	1.6
	80	97	9.6	32.0	2.3
Durion	10	722	28.1	7.2	1.3
	50	385	18.8	14.7	2.0
	80	144	13.9	30.5	2.9

[a] Calculated from the area under the tensile load/elongation curve.

The AEMWE performance of HTMA-DAPP and SES-TMA-1.7 AEMs was compared. For this study, we used identical MEA components except for the AEMs. Because the HTMA-DAPP AEM is more conductive than SES-TMA-1.7 (90 vs. 61 mS/cm in OH^- form), we used a 50% thicker HTMA-DAPP AEM to offset the difference in cell resistance. **Figure 3** shows the polarization curves of the two cells at 60 °C under deionized (DI) water-fed conditions. The two MEAs exhibited comparable performance where a thicker HTMA-DAPP AEM (wet thickness: 50 μm) was used. In a separate impedance measurement, the cell resistance of the HTMA-DAPP cell was 0.125 Ω cm^2 slightly higher than that of the SES-TMA cell (0.101 Ω cm^2). The result is consistent with the slightly higher area specific resistance (ASR) of the HTMA-DAPP AEM (0.056 Ω cm^2) than that of the SES-TMA-1.7 (0.052 Ω cm^2) estimated from the ex-situ hydroxide conductivity and membrane thickness in **Table 2**.

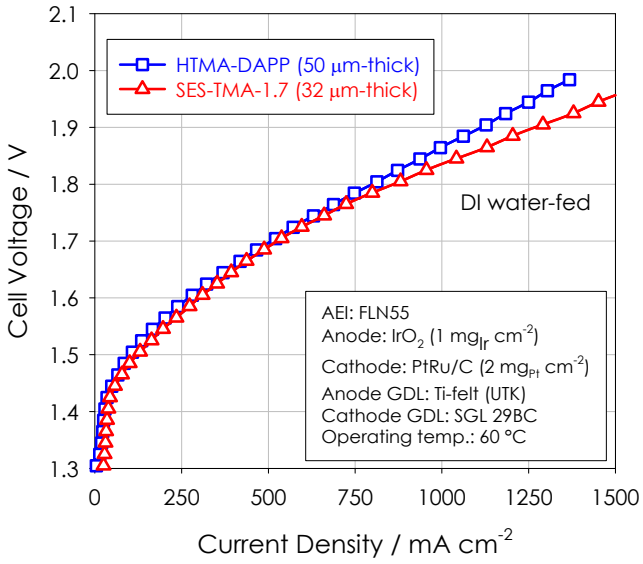

Figure 3. Performance comparison of AEMs in AEMWE cells (active area: 5 cm^2) using the HTMA-DAPP and SES-TMA-1.7 AEM under DI water-fed conditions.

In the previous work,[11] we investigated the impact of mechanical property on AEMWE durability under differential pressure conditions. For the durability test, a thicker version of the HTMA-

DAPP AEM (t = 78 μm) vs. SES-TMA-1.7 AEM (t = 53 μm) was used. The ASR of the two carbonated form AEMs was comparable (0.34 Ω cm^2 for HTMA-DAPP and 0.31 Ω cm^2 for SES-TMA-1.7). **Figure 4a** shows the voltage changes of the two cells at a constant current density of 500 mA cm^{-2} and a differential pressure of 100 psig. For the first trial of the MEA with the SES-TMA-1.7 AEM (red dash line), we obtained a high cell voltage (~ 2.1 V) during the first 7 hours. After re-applying the 100 psig differential pressure, the voltage was stabilized to ~ 2.0 V. The voltage kept increasing until a sudden pressure drop occurred at ~50 hours. The voltage degradation rate between 8 and 50 hours was ca. 200 μV h^{-1}. The post-operation analysis indicated that the cause of the voltage drop was an electronic short across the MEA. To confirm the instability of the SES-TMA-1.7 MEA under the differential pressure conditions, we prepared the identical cell and tested it again. Like the first trial, the second SES-TMA cell exhibited an initial voltage jump to ~2.1 V for the first 30 hours. After the first 30 hours, the voltage of the SES-TMA-1.7 MEA slowly increased at the voltage degradation rate of 310 μV h^{-1} until a slight voltage loss occurred at 70 hours, which might be a soft short (electrodes pressed through the membrane). The MEA underwent another voltage fluctuation at 200 hours in which the differential pressure dropped to < 20 psig. The cell could not hold the differential pressure and the cell voltage fluctuated after 200 hours. These experiments indicate that the durability of MEAs employing the SES-TMA AEM is not good under the differential pressure conditions. Next, we performed the durability test with a cell employing HTMA-DAPP AEM. Unlike the SES-TMA-1.7 AEM cell, we did not observe initial voltage jump. Due to the absence of the initial voltage jump, the cell employing HTMA-DAPP AEM could operate at approximately 100 mV lower voltage. The HTMA-DAPP cell showed stable voltage over 500 hours with much lower voltage degradation rate (50 μV h^{-1}). The durability of the HTMA-DAPP cell was further evaluated after the 500 hour-

test (**Figure 4b**) and the operating temperature increased to 65 °C for 170 hours. The voltage degradation rate during the 65 °C portion of the test increased to 200 μV h^{-1}. Next, the cell's temperature was returned to 50 °C for an additional 100 hours of runtime. The cell voltage increased from 1.98 to 2.07 V due to the drop in temperature, but the voltage degradation rate during the last 100 hours was low (< 50 μV h^{-1}) and the cell maintained its integrity at the 100 psi differential pressure throughout the test.

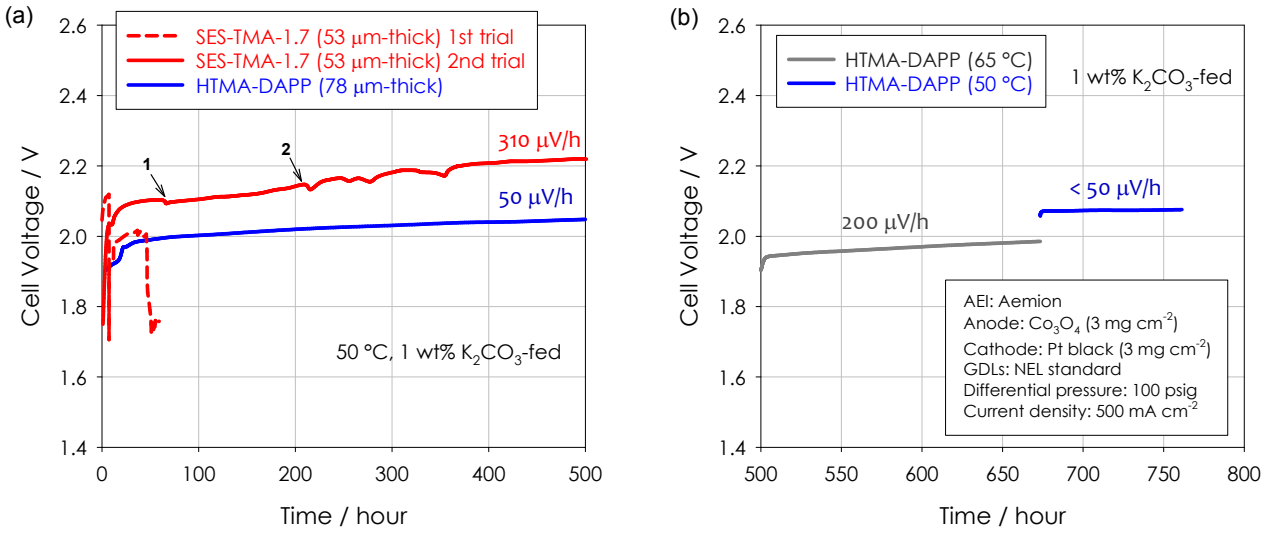

Figure 4. (a) Durability comparison between HTMA-DAPP and SES-TMA-1.7 AEMs in MEAs (active area: 28 cm^2). (b) Extended-term test after 500-hour test for the HTMA-DAPP cell. The AEMWE durability was evaluated using the commercial Aemion AEI. The data were redrawn from Ref. [11].

The MEA evaluation results suggest that the performance of the cells using the HTMA-DAPP and SES-TMA AEMs may be comparable when the lower conductive SES-TMA AEM is compensated with a thinner AEM. We did not observe a substantial chemical structural effect on the AEMWE's initial performance or interfacial delamination between the AEMs and dissimilar AEIs. However, the 53 μm-thick SES-TMA-1.7 AEM cannot withhold the 100 psig differential pressure due to its low strength and modulus. In contrast, the AEMWE cell using 78 μm-thick HTMA-DAPP can operate for > 750 hours under the differential pressure conditions. A thicker version of SES-TMA

AEM may withhold the differential pressure, but a lower hydrogen production efficiency is expected by an increased cell resistance.

Selection of anion exchange ionomers and their properties

Anion exchange ionomers (AEIs) for alkaline electrolyzers require good chemical stability, high hydroxide conductivity, electrochemical stability, low water uptake, and minimal interaction with electrocatalysts.[43] Good chemical stability of AEIs under high pH conditions can be achieved with pendant alkyl ammonium or other alkaline stable cationic group functionalized aryl ether-free polymers as we discussed in the previous section. From the hydroxide conductivity point of view, several factors including IEC, morphology, water uptake, and basicity of the cation hydroxide impact. Polyolefinic ionomers can have higher IEC (> 3 mequiv./g) due to the simpler polymer backbone structure. Our previous report suggested that high IEC polyolefinic ionomers allow high AEMWE performance (2.7 A cm^{-2} at 1.8 V),[14] however, the high IEC and water uptake may adversely impact AEMWE's durability.[11] Therefore, reducing the water uptake of polyolefinic ionomers is critical to obtain both good performance and durability of AEMWEs.[44] Polyaromatic ionomers exhibit a higher hydroxide conductivity than polyolefinic ionomers at a given water uptake and are therefore preferable for AEMWEs. Electrochemical stability is another critical requirement for AEIs as AEIs are exposed oxygen environment or high electrochemical potential. One critical issue related to the electrochemical stability is phenyl oxidation of ionomers at the anode; phenyl groups in the backbone of polyaromatic ionomers can be electrochemically oxidized to phenol at high electrode potentials (> 1.6 V vs. RHE).[45] The phenyl oxidation is detrimental because the phenol products are acidic (pK_a = 7.6 - 9.6) and are difficult to remove from the catalyst-ionomer interface. The acidic phenols neutralize the quaternary ammonium hydroxide thus decrease the activity of oxygen evolution reaction (OER) catalysts. To investigate this effect,

we selected three polyaromatic ionomers. The first AEI is a HTMA-DAPP which has several *ortho*-, *meta*- and *para*-substituted phenyl groups in the polymer backbone (**Figure 1b**). The second AEI is an alkyl trimethyl ammonium functionalized poly(fluorene) (FLN55). The FLN55 AEI was prepared by acid-catalyzed Friedel-Crafts polycondensations of 1,1,1-trifluoroacetone and fluorene monomers and subsequent amination with trimethylamine.[35] The quaternized poly(fluorene) has a central fused five-membered ring between two phenyl-groups providing non-rotating characteristics that lowers phenyl adsorption energy on electrocatalysts. The third AEI is a hexamethyl-*p*-terphenyl poly(benzimidazolium) (HMT-PMBI)[46], which is commercially available (Aemion AEI™, Ionomr)[47]. Unlike the HTMA-DAPP and FLN55 AEIs which have tethered alkyl ammonium cationic groups, the HMT-PMBI ionomer has a benzimidazolium cationic group in its backbone. The chemical structures of AEIs are shown in **Figure 1b**.

Table 4. Electrochemical properties of the selected AEIs used for this study

Cationic group	AEI	IEC [a] (mequiv./g)	WU [a] (%)	σ_{OH^-}, (mS cm^{-1})		% IEC change after alkaline stability test
				Liquid water (30 °C)	Vapor water (95% RH)	
Alkyl ammonium	HTMA-DAPP [b]	1.5	58	73	20, (80 °C)	8
Alkyl ammonium	FLN55 [c]	2.5	180	110	Not available	2.4
Benzimidazolium	HMT-PMBI [d]	2.1 - 2.5	35	> 80	23, (30 °C)	6

[a] measured with OH form membranes
[b] tested for 500 hours of 4 M NaOH treatment at 80 °C. Data were taken from Ref.[41].
[c] tested for 500 hours of 1 M NaOH treatment at 80 °C. Data were taken from Ref.[35].
[d] tested for 168 hours of 2 M NaOH treatment at 80 °C. Data were taken from Ref.[46].

Table 4 shows the IEC and other properties of the selected AEIs. The FLN55 AEI has a higher IEC (2.5 mequiv. g^{-1}) than that of the HTMA-DAPP AEI (1.5 mequiv. g^{-1}). The water uptake of the FLN55 AEI is much higher (180%), probably because the IEC of the ionomer passes the percolation threshold. Owing to the high IEC and water uptake, the FLN55 AEI has a higher hydroxide conductivity. The commercial HMT-PMBI ionomer has a relatively high IEC (2.1 - 2.5 mequiv. g^{-1}). The water uptake is relatively low primarily because of its low fractional free volume

297 due to polymer backbone functionalization.[48] The alkaline stability of all selected AEIs is good, <
298 10% change of IEC for several hundreds of hours in highly concentrated NaOH solutions at 80 °C.

299 Next, we compared the performance of AEMWEs using the HTMA-DAPP and FLN55 AEIs at 60
300 °C under DI water and 0.1 M NaOH-fed conditions (**Figure 5**). For this study, we prepared two
301 identical MEAs except for the ionomeric binders. We chose an SES-TMA AEM. The SES-TMA
302 AEM only has phenyl groups on the side chain, which has lower adsorption energy (-1.95 eV) than
303 bi- or ter-phenyl groups in the polymer backbone (-2.87 to -3.94 eV), which can minimize the
304 adverse impact of phenyl adsorption.[49] We tested the cells without differential pressure for this
305 case to prevent any premature membrane failure by differential pressure. Under DI-water-fed
306 conditions, the MEA using the FLN55 AEI exhibited much higher performance than using the
307 HTMA-DAPP AEI. Under 0.1 M NaOH-fed conditions, the MEA using the FLN55 AEI still
308 exhibited higher performance, but the performance differential was smaller. There are two possible
309 reasons for the higher performance of the FLN55 AEI. The first is the higher IEC of FLN55, which
310 can provide a higher pH environment at the catalyst-ionomer interface. This is beneficial to water
311 splitting catalytic activities, particularly to the OER. The second possible reason is related to the
312 electrochemical oxidation of the phenyl groups. Because HTMA-DAPP has a higher phenyl
313 adsorption energy on the IrO_2 OER catalyst, a higher rate of phenyl oxidation is expected.[45]
314 Although no systematic study was performed to determine which factor is predominant, a closer
315 look at the polarization curves suggests that phenyl oxidation may be the primary cause for the
316 lower performance of the HTMA-DAPP-bonded MEA. The kinetic performance of the HTMA-
317 DAPP-bonded electrodes was higher (**Figure 5a** inset), followed by a decrease in performance as
318 the operating cell voltage increased. Higher performance loss at a high cell voltage is a footprint
319 of phenyl oxidation, as the electrochemical phenyl oxidation rate increases with cell voltage. In

contrast, the kinetic performance of the highly conductive FLN55 AEI-bonded electrodes is similar to that of the HTMA-DAPP AEI-bonded electrodes, suggesting the ionomer IEC effect may be relatively small. The second indirect evidence comes from the electrolyzer performance under 0.1 M NaOH-fed conditions (**Figure 5b**). For the HTMA-DAPP-bonded electrodes, circulating an alkaline solution in the cell helps to neutralize acidic phenol compounds due to phenyl oxidation besides an increased electrolyte-catalyst surface area with the additional liquid electrolyte. Therefore, the performance improvement for the HTMA-DAPP-bonded electrodes is more significant under 0.1 M NaOH-fed conditions.

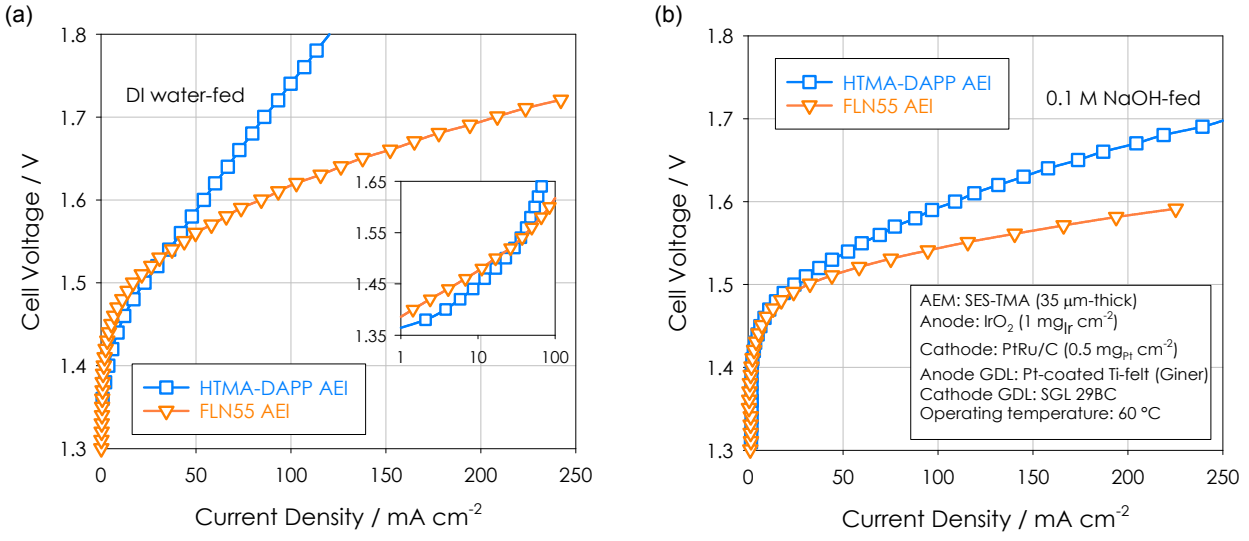

Figure 5. Performance comparison of AEMWE cells (active area: 5 cm^2) using the SES-TMA-1.4 AEM and two different AEIs under (a) DI water- and (b) 0.1 M NaOH-fed conditions. The active area of the

To confirm the adverse impact of phenyl oxidation on AEMWE performance, we further examined the voltage behaviors of the two AEI-bonded cells during a short-term test. If phenyl oxidation causes the performance loss, the AEMWE performance should gradually decrease as the phenyl oxidation at the catalyst-ionomer interface continuously proceeds during the short-term test.[50] **Figure 6** compares the cell voltage change over time for two identical cells except for the ionomeric binders. The cell using the HTMA-DAPP AEI exhibited a gradual increase in cell

voltage over the first 100 hours, while the cell using the FLN55 AEI was stable. This result confirms that phenyl oxidation of the HTMA-DAPP AEI is the major cause of the low performance and voltage degradation over time.

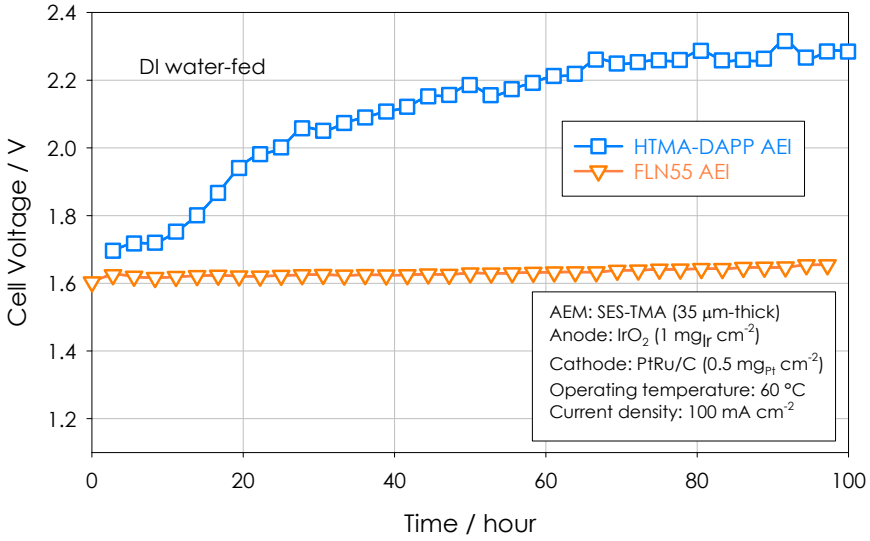

Figure 6. The comparison of cell voltage change of pure water-fed AEMWEs (active area: 5 cm^2) using the SES-TMA-1.4 AEM and two different AEIs.

The impact of phenyl adsorption was further investigated with a perovskite OER catalyst. In our previous study, the phenyl adsorption energy parallel to the surface of a perovskite catalyst, $La_{0.85}Sr_{0.15}CoC_3$, was much lower (-0.18 eV at 1.6 V) than that of the IrO_2 OER catalyst (-2.19 eV).[45] **Figure 7** shows the performance of perovskite OER catalyzed AEMWEs using HTMA-DAPP and FLN55 AEIs. It should be noted that perovskite OER catalyzed cells have a smaller performance differential than the IrO_2 OER catalyzed cells (**Fig. 5a**). This stems from the decreased phenyl group adsorbing characteristics of the perovskite catalyst. Note that the PGM-free catalyzed cell using the HTMA-DAPP AEI performed better than the IrO_2-catalyzed cell using the HTMA-DAPP AEI while the IrO_2-catalyzed cell performed better than the perovskite catalyzed cell when the FLN55 AEI was used. This result indicates that the adverse impact of phenyl adsorption can be mitigated by using less phenyl-adsorbing perovskite OER catalysts.

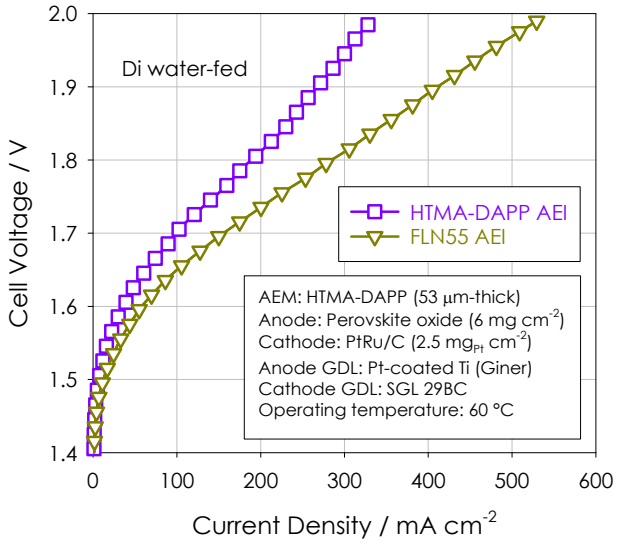

Figure 7. Performance comparison of the AEMWE cells (active area: 5 cm^2) using the HTMA-DAPP and FLN55 AEIs under Di water-fed conditions.

We further investigated the ionomer effect using the HTMA-DAPP AEM. **Figure 8** shows the same tendency; the cell with FLN55 AEI outperforms the cell with HTMA-DAPP AEI under both DI water- and 0.1 M NaOH-fed conditions. This result confirms that the FLN55 AEI is superior to the HTMA-DAPP AEI. The AEMWE performance was also compared with a polystyrene-based polyolefinic AEI, TMA53, which showed high performance in a previous report.[14] Under DI water-fed conditions, the cell with the TMA53 AEI showed a slightly better kinetic performance at low cell voltages (< 1.7 V) than the FLN55 AEI, indicating little, if any, adverse effect by side-chain phenyl oxidation for the TMA53-bonded cell. Under 0.1 M NaOH-fed conditions, however, the cell with the TMA53 AEI did not substantially increase. Under NaOH-fed conditions, the FLN55-bonded cell showed comparable performance to the cell with the TMA70 AEI, which was one of the best performances in AEMWEs reported so far.[14] Smaller improvement of the TMA-based AEIs is probably due to low polymer density and high water uptake (WU > 300%) of the polyolefinic ionomers. The relatively high volume of the polyolefinic ionomers can make large-area contact with the electrocatalysts which results in relatively small performance improvement

with flowing liquid electrolytes. While the TMA-based AEIs showed high performance under the pure water-fed conditions, the durability of AEMWEs using the TMA ionomers was limited to less than 200 hours at 60 °C due to the ionomer detachment from the electrocatalysts.[14] Therefore, this AEI study concludes that the FLN55 AEI is the most affordable option among available AEIs, although the TMA-based AEIs have potential to show better performance to that of the FLN55 AEI. Controlling water uptake of the TMA-based AEIs remains a technical challenge for durable AEMWE operation.

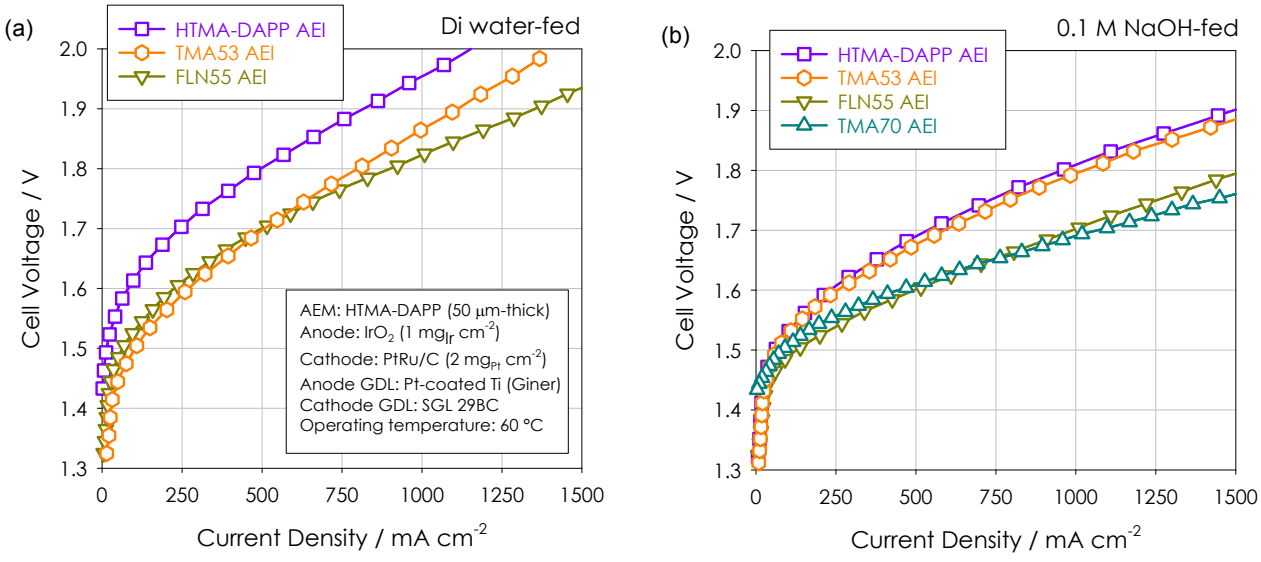

Figure 8. Performance comparison of AEIs in MEAs (active area: 5 cm^2) using the HTMA-DAPP AEM (a) AEMWE cells using the HTMA-DAPP, TMA53, and FLN55 AEIs under DI water-fed conditions (b) AEMWE cells using the HTMA-DAPP TMA53, FLN55, and TMA70 AEIs under 0.1 M NaOH-fed conditions.

Performance and durability of AEMWEs using down-selected polymer electrolytes

In this section, we compare the performance and durability of the down-selected HTMA-DAPP AEM and FLN55 AEI with commercially available materials in MEAs at a differential pressure of 100 psig. **Figure 9** compares the polarization curves of MEAs with three different combinations of AEMs and AEIs, HTMA-DAPP AEM/FLN55 AEI, Durion AEM/FLN55 AEI, and Durion AEM/Aemion AEI under DI water, 1 wt% K_2CO_3, and 1 wt% KOH-fed conditions. Here, we used a PGM-free anode catalyst (Co_3O_4) instead of an IrO_2 catalyst since cobalt-based catalysts are

known for their high catalytic activity and stability. Since cobalt possess *d*-band electrons similar to precious metals, the orbits grant more active sites for electrocatalytic water splitting.[51] The AEMWE's performance increased as DI water was replaced by 1 wt% K_2CO_3 then KOH. The MEA with the Durion AEM were to compare the difference between the FLN55 and Aemion AEIs. Under all of the electrolyte-fed conditions, the FLN55 AEI showed superior performance to the Aemion AEI. The cell voltage of the FLN55 AEI-bonded electrolyzer at 500 mA cm^{-2} was 2.13 V under DI water-fed conditions, which was 150 mV lower than the Aemion-bonded AEMWEs (2.28 V). The performance difference between the two MEAs narrowed to 80 mV under 1 wt% K_2CO_3-fed conditions (1.94 V for FLN55 vs. 1.86 V for Aemion). The performance difference further decreased to 30 mV at 500 mA cm^{-2} under 1 wt% KOH conditions (1.80 V for FLN55 vs. 1.83 V for Aemion). Considering that the IEC of both AEIs are similar, the performance loss is likely due to the electrochemical oxidation of the phenyl groups of the HMT-PMBI backbone. These studies indicate that using the FLN55 AEI, with non-rotating phenyl groups in their polymer backbone (reduces phenyl adsorption) has a performance benefit over the imidazolium-functionalized polyphenylene AEIs[52]. Next, we compared the performance of the reinforced Durion AEM with the HTMA-DAPP AEM using the same FLN55 AEI. Under DI water-fed conditions, the HTMA-DAPP and Durion cells displayed similar performance. The ASR of the HTMA-DAPP and Durion AEMs calculated from the hydroxide conductivity and AEM thickness are 0.055 and 0.034 Ω cm^2, respectively. Therefore, much superior performance of the Durion cell is expected. A possible reason for the relatively low performance of the Durion cell may be related to the electrochemical oxidation of the AEM due to a different backbone structure between the HTMA-DAPP and Durion AEMs. The backbone structure of HTMA-DAPP is composed of biphenyl and *ortho*-terphenyl at 1:2 ratio. Consequently, the backbone of HTMA-DAPP has a relatively lower phenyl adsorption

energy (-2.87 eV for biphenyl and -1.52 eV for *ortho*-terphenyl). The *m*-TPN1 in the reinforced Durion AEM is composed of *meta*-terphenyl which has a high phenyl adsorption energy of -3.61 eV.[49] Although the phenyl group in the AEM has a lower chance to make contact with catalysts, we could not rule out the electrochemical oxidation of AEMs because complete separation of the AEM effect is difficult.[11] When the electrolyte was changed from DI water to 1 wt% K_2CO_3 then to 1 wt% KOH solution, the performance of the Durion cell became slightly better than that of the HTMA-DAPP cell, suggesting that the acidic phenol of the *m*-TPN1 was effectively neutralized by the liquid electrolytes.

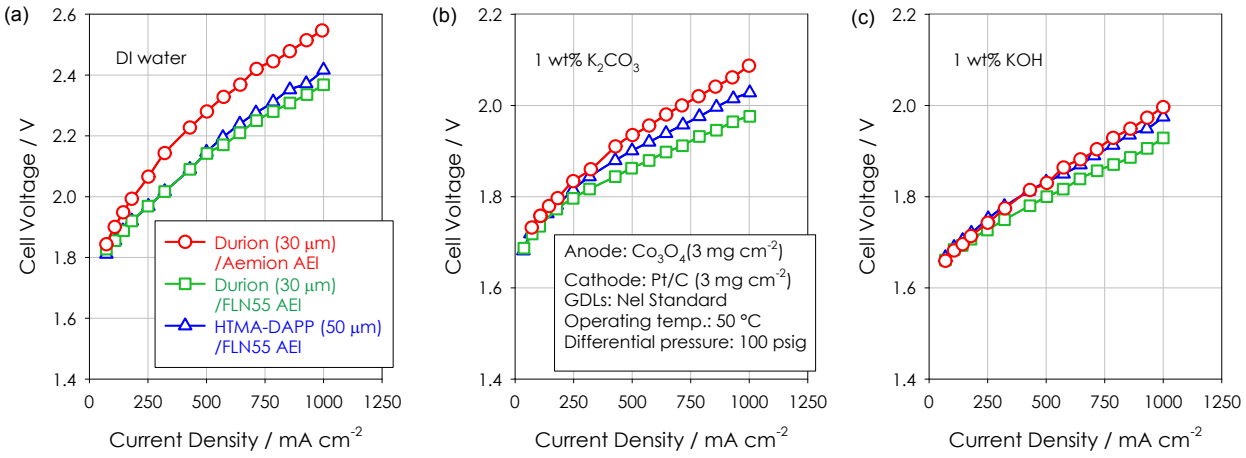

Figure 9. Performance comparison down-selected MEAs (active area: 28 cm^2) with commercial AEM and AEI. The AEMWE performance was measured under (a) DI water, (b) 1 wt% K_2CO_3 and (c) 1 wt% KOH-fed conditions.

The durability of AEMWEs using an HTMA-DAPP AEM (t = 50 μm) was evaluated at a higher current density (750 mA cm^{-2}). For this evaluation, we used two control MEAs, commercial Durion AEM/Aemion AEI and Durion AEM/FLN55 AEI. The initial voltage and voltage degradation rate of the AEMWE with the MEA using Durion AEM and Aemion AEI were notably higher than those of the MEA using the Durion AEM and FLN55 AEI (**Figure 10**). This result was consistent with the performance of those MEAs obtained with the polarization curves in **Figure 9**; the performance of AEMWE using the Aemion AEI is limited by the electrochemical

oxidation of the phenyl group of the ionomer. The AEMWE cell using the Durion AEM and FLN55 AEI showed a voltage degradation rate (303 $\mu V\ h^{-1}$) for the first 100 hours. For the Durion cell, we reduced the differential pressure to 60 psig after the first 100 hours because H_2 crossover current density exceeds the safety limit. It was noted that the cell voltage decreased approximately 10 mV and the voltage degradation rate also decreased to 94 $\mu V\ h^{-1}$. The voltage behavior of the AEMWE using the HTMA-DAPP AEM and FLN55 AEI was examined. The initial voltage (1.92 V) was similar to the AEMWE cell using the HTMA-DAPP AEM and the Aemion AEI (**Figure 4a**). The initial voltage degradation rate of the HTMA-DAPP cell was 274 $\mu V\ h^{-1}$, slightly lower than that of the Durion cell (303 $\mu V\ h^{-1}$). The lower voltage degradation rate of the HTMA-DAPP cell is consistent with the fact that the backbone of HTMA-DAPP is composed of phenyl groups with less adsorption energy. Although the contact between the AEM and Co_3O_4 electrocatalyst may be much less than the contact between AEI and Co_3O_4 electrocatalyst, it still impacts the performance and durability of AEMWEs. This may be further related to the dissolution of catalyst nanoparticles in quaternary ammonium polymers which creates a new interface between the AEM and the OER catalyst over time. For the HTMA-DAPP cell, we continued the durability testing at the differential pressure of 100 psig. There were two voltage-jumps for the HTMA-DAPP cell at the time of ~290 and 380 hours caused by the incidental system shut down. The cell voltage after the voltage jumps was stabilized like the control MEA with the Durion AEM and FLN55 AEI. However, the HTMA-DAPP cell stopped operating at 440 hours. It was noted that the differential pressure was held until catastrophic cell failure which was in stark contrast with the SES-TMA cell shown in **Figure 4a**. This is probably because the AEM failure of the HTMA-DAPP cell occurred with AEM rupture while the polyolefinic SES-TMA AEM likely failed due to creep rupture from the differential pressure over a prolonged period (**Figure 4a**). This durability

evaluation indicates that the 50 μm thickness of non-reinforced HTMA-DAPP AEM is not enough to hold the differential pressure while the 78 μm-thick HTMA-DAPP AEM cell operated for > 750 hours under the same differential pressure conditions.

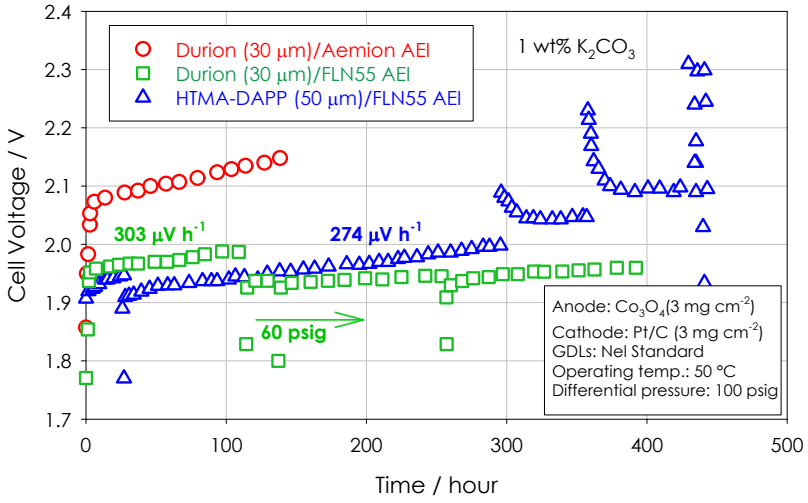

Figure 10. Durability comparison between HTMA-DAPP and Durion AEMs in MEAs (active area: 28 cm^2). The AEMWE durability was evaluated at 750 mA cm^{-2}.

PERSPECTIVES AND CONCLUDING REMARKS

In terms of AEMWE performance, we found that AEIs play a more significant role than AEMs, with little performance differences between various polymer architectures utilized in the AEMs. However, polymer backbone structure of AEIs was found to have a remarkable influence to AEMWE performance. This is reasonable because AEMWE performance is primarily determined by catalytic activity of hydrogen evolution reaction (HER) and OER, which are greatly influenced by ionomer-catalyst interactions. We demonstrated that FLN55 was less prone to phenyl adsorption improved cell performance. However, one may argue that the performance improvement is highly dependent upon catalysts and experimental conditions. For example, perovskite OER catalysts have less phenyl adsorption energy, less pH dependence on OER activity therefore polyaromatic ionomers may work well under pure water-fed conditions. In addition,

flowing highly concentrated NaOH solution provides additional hydroxide conduction pathways and makes the adverse impact of electrochemical oxidation of phenyl group in ionomeric binder on AEMWE performance not critical. Polyolefinic AEIs have great potential to be used as high-performance ionomers since these polymers do not have phenyl groups in their polymer backbone. However, relatively lower hydroxide conductivity at a given IEC may require more cationic functional groups which often result in excessive swelling and reduces the catalyst binding capacity. It has been known that excessive swelling of ionomers can make catalyst particles detach during AEMWE operation, particularly, under high current density operation.[14, 44] Therefore, it becomes critical to control the water uptake of polystyrene-based polyolefinic ionomers for the practical use of AEMWEs.

As for AEMs, we did not observe a negative impact of alkaline instability of the chosen AEMs on AEMWE performance. This is primarily because the currently available AEMs have good alkaline stability by adopting aryl ether-free polymer backbone and alkaline stable cationic functional groups. Alkaline stability of AEMs can be more critical for longer-term operation (> 1,000 hours) or circulating more concentrated alkaline electrolytes. The hydroxide conductivity of AEMs, on the other hand, can impact AEMWE performance. Since a practical AEMWE system requires differential pressure operation, relatively thick AEMs compared to the fuel cell system are used and can significantly reduce the hydrogen generation rate. In such case, using poly(phenylene) AEMs is beneficial as they have relatively higher conductivity than polyolefinic AEMs at a given IEC. One should note that this is a slightly different situation with AEM fuel cells where the low cell resistance can be obtained with a thin AEM (< 20 μm thick). For AEMWEs under differential pressure conditions, minimum thickness (> 50 μm) is required to hold the pressure, and hydroxide conductivity becomes more critical for the device performance.

In terms of AEMWE durability, the mechanical properties of AEMs are one of the most critical factors under differential pressure conditions. Our study indicates that the AEM strength and modulus that resist the differential pressure are more important than elongation. AEMs with low strength and modulus may yield their mechanical integrity during differential pressure operation and cannot hold pressure. We did not investigate AEMWE durability under ambient pressure or equal pressure conditions so it is difficult to conclude whether AEMs with low strength and modulus are not suitable for AEMWE applications. However, for differential pressure operation, it is clear that AEMs with low strength and modulus need high thickness or reinforcement for stable operation. This is consistent with PEM water electrolyzers that use elastomeric PFSA membranes which are relatively thick (> 100 μm) for differential pressure operation. However, due to the relatively low conductivity of AEMs, increasing the thickness of AEMs is more detrimental to performance. For poly(phenylene) AEMs that have high strength and modulus, catastrophic failure during differential pressure operation is a concern. Therefore, a thicker membrane is still favorable. In our study, 78 μm-thick quaternized poly(phenylene) membrane enabled > 700 hours under 100 psig (6.9 bar) differential pressure without failure. Reinforcement is a plausible approach to increase AEM's strength and modulus at lower thickness. We have shown that a PTFE-reinforced poly(phenylene) AEM (30 μm-thick) can operate for ~ 400 hours at ≥ 60 psig differential pressure without failure. However, further enhancement of mechanical properties or the use of thicker membrane may be required for a practical differential pressure level (20 - 50 bar).

Our results showed that the voltage degradation rate of well-performing AEMWEs was higher during the first ~100 hours than at a later stage of the durability test. The origin of the initial voltage increase was not fully investigated in this paper and is believed related to the phenyl group

oxidation of AEM that contacts catalyst particles. Our previous study shows that the initial voltage increase can be minimized by using a polyolefinic AEM.[11] Although chemical stability of AEMs under high pH conditions is one of the most critical factors for AEMWE durability, more studies are needed for minimizing the electrochemical instability of AEMs. As more mechanically and electrochemically stable AEMs are developed, decreasing gas permeability may become critical for AEM studies. The low gas permeability requirement was manifested with the thin reinforced Durion AEM which exhibited high hydrogen crossover current, thus the differential pressure needs to be reduced to 60 psig during the durability test in spite of the fact that no differential pressure related catastrophic failure was observed. Overall, AEMWE operation under high differential pressure conditions is technically more challenging than expected as multiple degradation pathways can be initiated. The electrochemical oxidation of phenyl group in AEM or AEI gives influence on AEMWE durability. The gradual performance loss by the electrochemical oxidation of polymer electrolytes is unrecoverable and appears notably at the first hundreds of hours of operation. Additionally, we observed that a higher operating temperature is detrimental to AEMWE durability. As the operating temperature increased from 50 to 65 °C, the voltage degradation rate increased from 50 to 200 $\mu V\ h^{-1}$. This result suggests that the current high-performance of AEMWEs at 80 °C or higher may not be a practical operating temperature as a much higher voltage degradation rate is expected. When compared with AEM fuel cells, the performance loss mechanisms of AEMWEs are different. The voltage stability of AEM fuel cells at a constant current density is strongly affected by limited hydrogen transfer at the anode in which liquid water is generated to limit reactant hydrogen access, i.e., flooding. For AEMWEs, there is no flooding-derived mass transport issue because liquid water is reactant. However, voltage degradation due to electrochemical oxidation of anode materials is much more significant as

AEMWEs operate at a much higher anode potential. In addition, limited reactant water transport by evolving gas is problematic for high current density operation. Although we have not discussed this issue in this manuscript, substantial AEMWE performance change can be made by the effective removal of gas bubbles or by using a high gas permeable AEI. Finally, the AEMWE's performance and durability are affected by circulating electrolytes and their interaction with AEM and AEI. We have not performed a thorough study in this aspect, but it is obvious as some examples shown in this study indicate a substantial difference in AEM performance depending on the type of electrolyte circulation. Circulating highly concentrated electrolyte may increase durability of AEMWEs since the ionomeric binders of most AEMWE systems are electrochemically unstable and circulating highly concentrated electrolyte can provide high hydroxide conductivity when ionomeric binders are degraded.

In conclusion, we emphasize here that the mechanical strength and modulus of AEMs needs to be considered in conjunction with the hydroxide conductivity to determine the longevity of the AEMWEs in practical operations of AEMWEs with high current density ($\geq$ 500 mA cm^{-2}) and differential pressure. Reinforced or poly(phenylene) AEMs are promising to meet the conductivity and mechanical property targets. The AEMs with high conductivity and mechanical properties further require low gas permeability that allows operating AEMWEs with relatively thin AEMs. The AEIs with the least catalyst-ionomer interaction are the most critical for AEMWE's performance. Our results indicate that phenyl oxidation of the cathode AEI is particularly detrimental, but other interactions such as cationic group adsorption[53] may also impact the AEMWE's performance. The phenyl oxidation should be understood both by the chemical structure factor of AEIs and also by the structural factors of electrocatalysts. Phenyl oxidation of AEMs can also occur at the beginning of the life test, although further studies may need to identify

the performance loss during the life test. In this study, poly(phenylene) AEMs with quaternized poly(fluorene) AEI showed the most promising AEMWE performance and durability for practical AEMWE operating conditions. The performance and durability of the demonstrated AEMWE are still inferior to state-of-the-art PEM electrolyzers, however, progress has been made by using a PGM-free anode catalyst and without compromising the advantageous zero-gap cell design of PEM electrolyzers. Further development of AEM electrolyzer systems may find a good place for AEMWE to generate green hydrogen in an economically viable pathway.

EXPERIMENTAL SECTION

Materials. Poly(styrene-butadiene-styrene) (SBS, 25 mol% styrene, 67 mol% 1,4-polybutadiene, 8 mol% 1,2-polybutadiene) was obtained from Kraton. *p*-Toluenesulfonyl hydrazide was purchased from Alfa Aesar. Tripropylamine, chlorobenzene, anhydrous toluene, anhydrous dichlorobenzene were purchased from Acros Organics. Triflic acid was purchased from Sigma-Aldrich. 7-Bromo-2-methylheptan-2-ol was prepared according to our previous report.[39] The commercial IrO_2 catalyst was purchased from Alfa Aesar (iridium(IV) oxide, Premion®, 99.99%, Ir 84.5% min). The PtRu/C catalyst (50 wt% Pt, 25 wt% Ru, HiSPEC® 121000) was purchased from Alfa Aesar. The Durion membrane (XION™ Composite – DURION AEM-215-30) was provided by Xergy. The Co_3O_4 was purchased from Alfa Aesar (20 – 30 nm, PN: 46347). Some testing involved a commercial platinum black while other tests used 50% Pt/C available from Tanaka (TEC10E50E). The commercial baseline ionomer was AP1-HNN8-00 from Ionomr. We purchased a platinum-coated titanium flow field for the anode of the 5 cm^2 cell and platinized titanium gas diffusion layers from Giner Labs. Ti-coated homemade GDL was provided by Professor Feng Yuan Zhang at the University of Tennessee at Knoxville. SGL 29 BC was used as the cathode GDL of 5 cm^2 cells.

Material Synthesis. SES-TMA was synthesized as follows. Poly(styrene-ethylene-styrene) (SES) was prepared by hydrogenation of poly(styrene-butadiene-styrene) (SBS) block copolymer with *p*-toluenesulfonyl hydrazide. Bromoakylation and quaternization of SES were conducted using a similar procedure to our previous report of SEBS.[39] HTMA-DAPP was prepared as described by Hibbs.[41, 54]. For the HTMA-DAPP AEI, HTMA-DAPP AEI was dispersed in dimethylacetamide (DMAc) (5 wt%). FLN-55 was prepared as described by Maurya et al.[35] For the FLN55 AEI, we used ethanol as the dispersing agent (5 wt%). TMA AEIs was prepared as described by Li et al.[14] Perovskite oxide $La_{0.85}Sr_{0.15}O_3$ was synthesized as described by Li et al.[45]

Conductivity of AEMs.

The ion conductivity (σ in mS cm^{-1}) of the AEMs (approximate size: 3 cm × 0.5 cm) was measured from AC impedance spectroscopy data using a Solartron 1260 gain phase analyzer. The AEMs were firstly converted to hydroxide or carbonate form right before the measurement. To convert to the hydroxide and carbonate form AEMs, the AEMs were immersed in 0.5 M NaOH and K_2CO_3 solutions, respectively at 80 °C for 90 min, followed by a thorough wash with DI water several times.

Measurements were carried out under fully hydrated conditions at 50 °C where the cell was immersed in deionized water that was decarbonized by boiling prior to use. The ionic conductivity was calculated according to the following equation:

$$\sigma \text{ (mS cm}^{-1}) = L / (R \times W \times T)$$

where L is the distance between the two inner Pt plates (1.456 cm), R is the resistance of the AEM in Ω, and W and T are the widths and the thickness of the AEM in centimeters, respectively.

Tensile Properties of AEMs.

The Tensile properties of the membranes were investigated using a TA Q800-RH DMA instrument. A sample size of 20 mm × 6 mm was used for all experiments. The samples were loaded in a testing chamber with a distance of 6 mm between the clamps and a preload of 0.02 N to prevent any film slack. Before conducting the tensile test, the environmental chamber was heated up to 50 °C at a rate of 0.7 °C min^{-1} and the relative humidity was increased to the desired value at a rate of 2 % RH min^{-1}. The membranes were then equilibrated at the desired conditions before the test. The films were equilibrated for 15 min when tested at 10% RH, and 30 min when tested at 80% RH. The tensile tests were performed at ramp stress of 5 MPa min^{-1}.

Electrolyzer Performance Test.

Laboratory-scale 5 cm^2 cell: For house-made AEMs, we first converted all AEMs to hydroxide form by immersing the AEMs in 1 M NaOH for two hours then rinsing them with Milli-Q water. For the catalyst ink, we mixed the AEI dispersion with the catalyst by sonication. The catalyst inks were painted onto the GDLs (5 cm^2; anode, titanium-based; cathode, SGL 29 BC) to make gas diffusion electrodes (GDEs). The prepared GDEs, AEM, and Teflon gaskets were assembled into a single cell with 60 inch-pounds torque. The cell was tested by a Biologic SP-200 potentiostat in combination with an HCV-3048 30 A/48 V power booster. The cell was first cycled between 1.3 V and 2.0 V at 20 mV s^{-1} while flowing 0.1 M NaOH solution (10 mL/min) on both the anode and cathode at 60 °C until the polarization curves stabilized. The alkaline solution was purged by flowing approximately 500 ml of Milli-Q water, then the polarization curve was recorded between 1.3 and 2.0 V at 20 mV s^{-1} while flowing Milli-Q water (10 mL/min) at 60 °C (**Figures 3, 5, 7,** and **8**). We ensure no residual alkaline solution by checking the effluent pH.

Laboratory-scale 28 cm^2 cell. We used commercial Co_3O_4 catalysts for the anode. First, 0.30 g Co_3O_4 (20 - 30 nm, Alfa Aesar, PN: 46347) was mixed with 1.6 g DI water, followed by 5.5 g

isopropyl alcohol. Lastly, 0.90 g of an AEI solution was added, which contained 3.5 wt% polymers. The solution was then mixed at room temperature with a magnetic stir bar and sonicated for 20 min (Q Sonica Q55, 20 kHz, amplitude = 25). This ink was then sprayed onto a heated porous titanium substrate (T = 80 °C) using bottled nitrogen. The loading was determined by the weight increase of the final dried part. The part was then cut down to a GDE of the proper size and used as the anode. The cathode was fabricated using the same ratio, but the catalyst was Pt black or Pt/C, as indicated in the text, and the substrate was carbon paper. The membrane was soaked in 60 °C DI water for 2 hours then ion-exchanged in 0.5 M NaOH for 1 hour. Next, using the exchanged membrane and the two GDEs, the cell stack was assembled in Nel's 28 cm² commercial hardware. The electrolyzer performance was measured with feeding DI water, 1 wt.% K_2CO_3 or 1 wt% KOH solutions (**Figure 9**). The water source was a 1 wt% liquid electrolyte solution that was circulated and topped off with DI water to make up for the water loss. The single cells were then run with current densities, temperatures, and pressures as indicated. The cell performance was measured after a few hours of operation to obtain steady-state performance.

Electrolyzer Durability Test.

For the durability test of 5 cm^2 cells shown in **Figure 6**, we applied a constant current (100 mA cm^{-2}) at ambient pressure while flowing DI-water (5 mL/min) in the anode. All tests using a 5 cm^2 cell were carried out at ambient pressure. In the 28 cm^2 durability tests shown in **Figure 10**, the cell stack was operated in an anode-only electrolyte feed configuration using 1 wt% K_2CO_3. The electrolyte/O_2 outlet stream from the cell stack was then recirculated into a holding tank where the O_2 was subsequently vented. As the water was consumed in the electrochemical reaction, fresh DI water was introduced into the system to maintain a constant volume. This flowing electrolyte was also heated to control the cell temperature. The test was run

in constant current mode with set points discussed in the text above. For differential pressure operation, the hydrogen pressure was controlled using a back pressure regulator. Crossovered H_2 was monitored by an H_2 sensor. The test was stopped when the crossovered H_2 exceeds the safety limit of the system.

ASSOCIATED CONTENT

AUTHOR INFORMATION

Corresponding Authors

*E-mail: yskim@lanl.gov (Y.S.K).

Author contributions

A. Motz & D. Li: data curation, formal analysis, investigation, methodology, validation and writing. A. Keane, L. D. Manriquez, S. Maurya, H. Chung, J. Jeon, & M. Pagels: Data curation, formal analysis and investigation. E. J. Park: data curation, formal analysis, investigation and writing. C. Fujimoto, C. Bae, K. E. Ayers: formal analysis, resources, supervision and writing. Y. S. Kim: conceptualization, formal analysis, funding acquisition, project administration and writing.

Conflicts of interest

There are no conflicts to declare.

ACKNOWLEDGEMENTS

We gratefully acknowledge research support from the HydroGEN Advanced Water Splitting Materials Consortium (Award Number: 2.2.0.401), established as part of the Energy Materials Network under the US Department of Energy, Office of Energy Efficiency and Renewable Energy, Hydrogen and Fuel Cell Technologies Office (HFTO). We thank Professors Yuehe Lin at Washington State University and Feng Yuan Zhang at University of Tennessee, Knoxville for

providing NiFe catalysts and Ti GDLs, respectively. We appreciate a donation of SBS block copolymer from Kraton. Durion AEMs were kindly provided by Bamdad Bahar, Xergy. Los Alamos National Laboratory is operated by Triad National Security, LLC under US Department of Energy Contract Number 89233218CNA000001.

REFERENCES

1. I. Staffell, D. Scamman, A. V. Abad, P. Balcombe, P. E. Dodds, P. Ekins, N. Shah and K. R. Ward, *Energy & Environmental Science*, 2019, **12**, 463-491.
2. S. A. Grigoriev, V. N. Fateev, D. G. Bessarabov and P. Millet, *International Journal of Hydrogen Energy*, 2020, **45**, 26036-26058.
3. O. Schmidt, A. Gambhir, I. Staffell, A. Hawkes, J. Nelson and S. Few, *International Journal of Hydrogen Energy*, 2017, **42**, 30470-30492.
4. K. E. Ayers, E. B. Anderson, C. B. Capuano, B. D. Carter, L. T. Dalton, G. Hanlon, J. Manco and M. Niedzwiecki, *ECS Transactions*, 2010, **33**, 3-15.
5. S. M. Saba, M. Muller, M. Robinius and D. Stolten, *International Journal of Hydrogen Energy*, 2018, **43**, 1209-1223.
6. B. Zayat, D. Mitra, A. Irshad, A. S. Rajan and S. R. Narayanan, *Current Opinion in Electrochemistry*, 2021, **25**, 030518.
7. L. Wang, T. Weissbach, R. Reissner, A. Ansar, A. S. Gago, S. Holdcroft and K. A. Friedrich, *ACS Applied Energy Materials*, 2019, **2**, 7903-7912.
8. H. A. Miller, K. Bouzek, J. Hnat, S. Loos, C. I. Bernacker, T. Weibgarber, L. Rontzsch and J. Maeier-Haack, *Sustainable Energy & Fuels*, 2020, **4**, 2114-2133.
9. H. Janssen, J. C. Bringmann, B. Emonts and V. Schroeder, *International Journal of Hydrogen Energy*, 2004, **29**, 759-770.
10. H. I. Lee, M. Mehdi, S. K. Kim, H. S. Cho, M. J. Kim, W. C. Cho, Y. W. Rhee and C. H. Kim, *Journal of Membrane Science*, 2020, **616**, 118541.
11. D. Li, A. R. Motz, C. Bae, C. Fujimoto, G. Yang, F.-Y. Zhang, K. E. Ayers and Y. S. Kim, *Energy & Enveronmental Science*, 2021, **14**, 3393-3419.
12. C. C. Pavel, F. Cecconi, C. Emiliani, S. Santiccioli, A. Scaffidi, S. Catanorchi and M. Comotti, *Angewandte Chemie-International Edition*, 2014, **53**, 1378-1381.
13. M. Bernt, J. Schroter, M. Mockl and H. A. Gasteiger, *Journal of the Electrochemical Society*, 2020, **167**, 124502.
14. D. Li, E. J. Park, W. Zhu, Q. Shi, Y. Zhou, H. Tian, Y. Lin, A. Serov, B. Zulevi, E. D. Baca, C. Fujimoto, H. T. Chung and Y. S. Kim, *Nature Energy*, 2020, **5**, 378-385.
15. J. Xiao, A. M. Oliveira, L. Wang, Y. Zhao, T. Wang, J. Wang, B. P. Setzler and Y. Yan, *ACS Catalysis*, 2021, **11**, 264-270.
16. M. R. Kraglund, M. Carmo, G. Schiller, S. A. Ansar, D. Aili, E. Christensen and J. O. Jensen, *Energy & Environmental Science*, 2019, **12**, 3313-3318.
17. P. Chen and X. Hu, *Advanced Energy Materials*, 2020, **10**, 2002285.
18. S. Gottesfeld, D. R. Dekel, M. Page, C. Bae, Y. Yan, P. Zelenay and Y. S. Kim, *Journal of Power Sources*, 2018, **375**, 170-184.
19. W. You, K. J. T. Noonan and G. W. Coates, *Progress in Polymer Science*, 2020, **100**, 101177.
20. N. Chen and Y. M. Lee, *Progress in Polymer Science*, 2021, **113**, 101345.

21. M. R. Hibbs, *Journal of Polymer Science Part B-Polymer Physics*, 2013, **51**, 1736-1742.
22. Z. Zhang, L. Wu, J. R. Varcoe, C. Li, A. L. Ong, S. Poynton and T. Xu, *Journal of Materials Chemistry A*, 2013, **1**, 2595-2601.
23. A. D. Mohanty and C. Bae, *Journal of Materials Chemistry A*, 2014, **2**, 17314-17320.
24. K. M. Hugar, H. A. Kostalik and G. W. Coates, *Journal of the American Chemical Society*, 2015, **137**, 8730-8737.
25. J. T. Fan, A. G. Wright, B. Britton, T. Weissbach, T. J. G. Skalski, J. Ward, T. J. Peckham and S. Holdcroft, *ACS Macro Letters*, 2017, **6**, 1089-1093.
26. M. G. Marino and K. D. Kreuer, *Chemsuschem*, 2015, **8**, 513-523.
27. J. S. Olsson, T. H. Pham and P. Jannasch, *Advanced Functional Materials*, 2018, **28**, 1702758.
28. J. Wang, Y. Zhao, B. P. Setzler, S. Rojas-Carbonell, C. Ben Yehuda, A. Amel, M. Page, L. Wang, K. Hu, L. Shi, S. Gottesfeld, B. J. Xu and Y. S. Yan, *Nature Energy*, 2019, **4**, 392-398.
29. C. Fujimoto, D. S. Kim, M. Hibbs, D. Wrobleski and Y. S. Kim, *Journal of Membrane Science*, 2012, **423-424**, 438-449.
30. C. G. Arges and V. Ramani, *Proceedings of the National Academy of Sciences of the United States of America*, 2013, **110**, 2490-2495.
31. A. D. Mohanty, S. E. Tignor, J. A. Krause, Y. K. Choe and C. Bae, *Macromolecules*, 2016, **49**, 3361-3372.
32. A. C. Yang-Neyerlin, S. Medina, K. M. Meek, D. J. Strasser, C. He, D. M. Knauss, W. E. Mustain, S. Pylypenko and B. Pivovar, *Journal of the Electrochemical Society*, 2021, **168**, 044525.
33. H. Ono, T. Kimura, A. Takano, K. Asazawa, J. Miyake, J. Inukai and K. Miyatake, *Journal of Materials Chemistry A*, 2017, **5**, 24804-24812.
34. N. U. Hassan, M. Mandal, G. Huang, H. A. Firouzjaie, P. A. Kohl and W. E. Mustain, *Advanced Energy Materials*, 2020, **10**, 2001986.
35. S. Maurya, S. Noh, I. Matanovic, C. H. Park, C. N. Vilarrubia, U. Martinez, J. Han, C. Bae and Y. S. Kim, *Energy & Environmental Science*, 2018, **11**, 3283-3291.
36. D. P. Leonard, S. Maurya, E. J. Park, S. Noh, C. Bae, E. D. Baca, C. Fujimoto and Y. S. Kim, *Journal of Materials Chemistry A*, 2020, **8**, 14135-14144.
37. Y. K. Choe, C. Fujimoto, K. S. Lee, L. T. Dalton, K. Ayers, N. J. Henson and Y. S. Kim, *Chemistry of Materials*, 2014, **26**, 5675-5682.
38. B. Motealleh, Z. Liu, R. I. Masel, J. P. Sculley, Z. R. Ni and L. Meroueh, *International Journal of Hydrogen Energy*, 2021, **46**, 3379-3386.
39. J. Y. Jeon, S. Park, J. Han, S. Maurya, A. D. Mohanty, D. Tian, N. Saikia, M. Hickner, C. Y. Ryu, M. E. Tuckerman, S. J. Paddison, Y. S. Kim and C. Bae, *Macromolecules*, 2019, **52**, 2139-2147.
40. W. H. Lee, E. J. Park, J. Han, D. W. Shin, Y. S. Kim and C. Bae, *ACS Macro Letters*, 2017, **6**, 566-570.
41. E. J. Park, S. Maurya, M. R. Hibbs, C. H. Fujimoto, K. D. Kreuer and Y. S. Kim, *Macromolecules*, 2019, **52**, 5419-5428.
42. S. Noh, J. Y. Jeon, S. Adhikari, Y. S. Kim and C. Bae, *Accounts of Chemical Research*, 2019, **52**, 2745-2755.
43. J. F. Zhang, W. K. Zhu, T. Huang, C. Y. Zheng, Y. B. A. Pei, G. Q. Shen, Z. X. Nie, D. Xiao, Y. Yin and M. D. Guiver, *Adv Sci*, 2021, **8**, 2100284.
44. G. Huang, M. Mandal, N. Ul Hassan, K. Groenhout, A. Dobbs, W. E. Mustain and P. A. Kohl, *Journal of the Electrochemical Society*, 2020, **167**, 164514.
45. D. Li, I. Matanovic, A. S. Lee, E. J. Park, C. Fujimoto, H. T. Chung and Y. S. Kim, *ACS Applied Materials & Interfaces*, 2019, **11**, 9696-9701.
46. A. G. Wright, J. T. Fan, B. Britton, T. Weissbach, H. F. Lee, E. A. Kitching, T. J. Peckham and S. Holdcroft, *Energy & Environmental Science*, 2016, **9**, 2130-2142.

47. P. Fortin, T. Khoza, X. Z. Cao, S. Y. Martinsen, A. O. Barnett and S. Holdcroft, *Journal of Power Sources*, 2020, **451**, 227814.
48. X. Y. Luo, D. I. Kushner, J. Li, E. J. Park, Y. S. Kim and A. Kusoglu, *Advanced Functional Materials*, 2021, **31**, 2008778.
49. I. Matanovic, S. Maurya, E. J. Park, J. Y. Jeon, C. Bae and Y. S. Kim, *Chemistry of Materials*, 2019, **31**, 4195-4204.
50. S. Maurya, A. S. Lee, D. Li, E. J. Park, D. P. Leonard, S. Noh, C. Bae and Y. S. Kim, *Journal of Power Sources*, 2019, **436**, 226866.
51. J. H. Wang, W. Cui, Q. Liu, Z. C. Xing, A. M. Asiri and X. P. Sun, *Advanced Materials*, 2016, **28**, 215-230.
52. V. Galvan, B. Shrimant, C. Bae and G. K. S. Prakash, *ACS Applied Energy Materials*, 2021, **4**, 5858-5867.
53. H. T. Chung, U. Martinez, I. Matanovic and Y. S. Kim, *The Journal of Physical Chemistry Letters*, 2016, **7**, 4464-4469.
54. M. R. Hibbs, *Journal of Polymer Science Part B: Polymer Physics*, 2013, **51**, 1736-1742.